European Journal of Nuclear Medicine and Molecular Imaging
https://doi.org/10.1007/s00259-022-05752-6

ORIGINAL ARTICLE

Unified spatial normalization method of brain PET images using adaptive probabilistic brain atlas

Tianhao Zhang[1,2] · Binbin Nie[1,2] · Hua Liu[1,2] · Baoci Shan[1,2] · Alzheimer's Disease Neuroimaging Initiative

Received: 4 November 2021 / Accepted: 1 March 2022

Abstract

Purpose A unique advantage of the brain positron emission tomography (PET) imaging is the ability to image different biological processes with different radiotracers. However, the diversity of the brain PET image patterns also makes their spatial normalization challenging. Since structural MR images are not always available in the clinical practice, this study proposed a PET-only spatial normalization method based on adaptive probabilistic brain atlas.

Methods The proposed method (atlas-based method) consists of two parts, an adaptive probabilistic brain atlas generation algorithm, and a probabilistic framework for registering PET image to the generated atlas. To validate this method, the results of MRI-based method and template-based method (a widely used PET-only method) were treated as the gold standard and control, respectively. A total of 286 brain PET images, including seven radiotracers (FDG, PIB, FBB, AV-45, AV-1451, AV-133, [^{18}F]altanserin) and four groups of subjects (Alzheimer disease, Parkinson disease, frontotemporal dementia, and healthy control), were spatially normalized using the three methods. The results were then quantitatively compared by using correlation analysis, meta region of interest (meta-ROI) standardized uptake value ratio (SUVR) analysis, and statistical parametric mapping (SPM) analysis.

Results The Pearson correlation coefficient between the images computed by atlas-based method and the gold standard was 0.908 ± 0.005. The relative error of meta-ROI SUVR computed by atlas-based method was $2.12 \pm 0.18\%$. Compared with template-based method, atlas-based method was also more consistent with the gold standard in SPM analysis.

Conclusion The proposed method provides a unified approach to spatially normalize brain PET images of different radiotracers accurately without MR images. A free MATLAB toolbox for this method has been provided.

Keywords PET · Brain imaging · Spatial normalization · Probabilistic brain atlas

Introduction

Positron emission tomography (PET) combined with a variety of radiotracers can image function, metabolism, neurochemistry, and pathology in the living human brain [1]. Meanwhile, new radiotracers for brain PET imaging have been continuously developed, expanding the application scope of brain PET imaging [2]. Spatial normalization is an essential procedure in objective assessment and statistical comparison of brain PET images. However, the different patterns of the brain PET images of different radiotracers make their spatial normalization challenging.

A widely used method of brain PET image spatial normalization is MRI-based method [3]. In this method, brain PET images and corresponding structural MR images (sMRI) need to be co-registered first, and then use sMRI as an intermediary to perform spatial normalization. Since the sMRI provides better anatomical information and spatial resolution than PET images, it is generally believed that the MRI-based method has high accuracy. However, in some clinical practice and many retrospective data, there is often no corresponding sMRI [4]. Additional MRI scans can also bring additional costs and risks for patients. Moreover, there

This article is part of the Topical Collection on Advanced Image Analyses (Radiomics and Artificial Intelligence).

✉ Baoci Shan
shanbc@ihep.ac.cn

[1] Beijing Engineering Research Center of Radiographic Techniques and Equipment, Institute of High Energy Physics, Chinese Academy of Sciences, Beijing, 100049, China

[2] School of Nuclear Science and Technology, University of Chinese Academy of Sciences, Beijing, 100049, China

Published online: 08 March 2022

are some patients who are contraindicated to undergo MRI scan due to the pacemakers and metal implants. These reasons highlight the significance of developing PET-only spatial normalization method.

The template-based method is a commonly used PET-only method which is based on minimizing the difference between the individual image and the template image with constraints on the plausibility of deformations. The accuracy of the template-based method depends on the similarity between the individual image and the template image. Therefore, different brain templates need to be constructed for different radiotracers, even the same radiotracers with different brain pathological states [5–7]. When the individual image and the template image are quite different, which is very common in pathological imaging (such as amyloid-β imaging and tau imaging), the template-based method will reduce the accuracy of spatial normalization and impair the results of the statistical analysis [8, 9].

To overcome these problems, we consider using the brain cytoarchitecture information as the prior information to spatially normalize brain PET images. For brain structural MR images, a spatial normalization algorithm named "unified segmentation," using the tissue probability maps of gray matter, white matter, and cerebrospinal fluid (CSF) as the prior information and unifying the spatial normalization, segmentation, and nonuniformity correction in a probabilistic framework of generative model, has been proposed [10]. However, due to diversity and complexity of the brain PET image patterns, the brain PET image signal intensity cannot be simply treated as the generation model of gray matter, white matter, and CSF. Instead, cytoarchitectonic maps may match the brain PET images since the PET is a molecular imaging that allows assessment of molecular processes at cellular level.

In this study, we developed a PET-only spatial normalization method based on the adaptive probabilistic brain atlas suitable for brain PET images with different tracers and brain diseases. The method will be referred as atlas-based method in the following. In atlas-based method, an adaptive probabilistic brain atlas was generated and combined with the unified segmentation algorithm to perform spatial normalization for each individual brain PET image. In order to verify this method, three methods (MRI-based method, template-based method, and atlas-based method) were used to perform spatial normalization for each of the brain PET images and the results of MRI-based method were treated as gold standard. The accuracy of this method was evaluated in three aspects. First, Pearson correlation coefficients between the spatially normalized images computed by the MRI-based method and those computed by the other two methods were computed. Second, the meta region of interest (meta-ROI) standardized uptake value ratios (SUVRs) of the healthy controls (HC), Alzheimer disease (AD), Parkinson disease (PD), and frontotemporal dementia (FTLD) brain PET images were calculated with the three methods, and the relative errors and the Pearson correlation coefficients between the meta-ROI SUVRs computed with MRI-based method and those computed with the other two methods were calculated. Third, the voxel-wise statistical parametric mapping (SPM) results between patients and HC obtained with the three methods were compared.

Materials and methods

Subjects and radiotracers

A total of 406 brain PET images, including FDG (^{18}F-fluro-2-deoxyglucose), PIB (^{11}C-Pittsburgh Compound B), FBB (^{18}F-Florbetaben), AV-45 (^{18}F-florbetapir), AV-1451 (^{18}F-flortaucipir), AV-133 (9-^{18}F-Fluoropropyl-(+)-dihydrotetrabenazine), and [^{18}F]altanserin (3-(2-(4-(4-[^{18}F] fluorobenzoyl)-1-piperidinyl)ethyl)-2,3-dihydro-2-thioxo-4(1H)-quinazolinone), and their corresponding T1-weighted MR images were included in this study and divided into two cohorts: a template creation cohort (120 images) and a registration validation cohort (286 images). All data come from the following five public databases, including ADNI (Alzheimer's Disease Neuroimaging Initiative; http://adni.loni.usc.edu), AIBL (The Australian Imaging, Biomarker and Lifestyle Study of Aging; http://www.AIBL.csiro.au), ICBM (International Consortium for Brain Mapping) [11], NIFD (Neuroimaging in Frontotemporal Dementia; https://memory.ucsf.edu/research-trials/research/allftd), and PPMI (Parkinson's Progression Markers Initiative; https://www.ppmi-info.org). Informed consent was obtained from all participants by the leading institutions of each dataset. The ethics committee of the leading institution of each dataset approved its study. The demographic information of the subjects is shown in Table 1. Imaging protocols are shown in Supplementary File 1.

MRI-based and template-based spatial normalization method

For MRI-based method, the PET images were first co-registered to their corresponding T1-weighted MR images by using a rigid-body model with the normalized mutual information as the objective function in SPM12 (Wellcome Trust Centre for Neuroimaging, London, UK). Then, the MR images were spatially normalized into MNI (Montreal Neurological Institute) space using SPM12 "Normalise" tool with defined settings. The deformation fields for MR image spatial normalization were then applied to the corresponding co-registered PET images. The matrix size of the spatially normalized images was $121 \times 145 \times 121$, and

Table 1 The demographic information of the subjects

Tracers	Cohort	Group	*n*	Sex (M/F)	Age (mean ± STD)	Databases
FDG	Registration validation	HC	30	15/15	78.1 ± 9.5	ADNI
		AD	28	17/11	76.4 ± 7.2	ADNI
		FTLD	18	12/6	62.5 ± 6.5	NIFD
	Template creation	HC	10	6/4	75.1 ± 5.1	ADNI
		AD	10	6/4	72.0 ± 7.6	ADNI
		FTLD	10	6/4	63.1 ± 3.6	NIFD
PIB	Registration validation	HC	15	9/6	78.1 ± 5.4	ADNI
		AD	15	9/6	73.9 ± 9.4	ADNI
		FTLD	8	6/2	64.3 ± 5.2	NIFD
	Template creation	Negative	10	5/5	74.3 ± 4.5	AIBL
		Positive	10	3/7	74.9 ± 7.4	AIBL
FBB	Registration validation	HC	14	5/9	70.1 ± 7.7	ADNI
		AD	21	15/6	74.7 ± 6.9	ADNI
		PD	26	20/6	65.2 ± 8.5	PPMI
	Template creation	Negative	10	2/8	70.3 ± 6.5	ADNI
		Positive	10	6/4	72.1 ± 8.6	ADNI
AV-45	Registration validation	HC	18	6/12	72.5 ± 7.9	ADNI
		AD	11	6/5	79.1 ± 5.3	ADNI
	Template creation	Negative	10	4/6	79.7 ± 8.7	ADNI
		Positive	10	7/3	71.9 ± 13.6	ADNI
AV-1451	Registration validation	HC	32	13/19	70.7 ± 7.7	ADNI
		AD	20	14/6	75.2 ± 6.6	ADNI
	Template creation	Negative	10	2/8	79.2 ± 6.9	ADNI
		Positive	10	8/2	72.2 ± 10.4	ADNI
AV-133	Registration validation	HC	5	5/0	66.3 ± 8.0	PPMI
		PD	15	12/3	63.0 ± 9.8	PPMI
	Template creation	PD	10	7/3	61.8 ± 12.7	PPMI
[^{18}F]altanserin	Registration validation	HC	10	5/5	26.6 ± 5.7	ICBM

the resolution was 1.5 × 1.5 × 1.5 mm. Same matrix size and resolution were used in template-based method and atlas-based method.

For template-based method, the templates were constructed by averaging the intensity normalized images in the template creation cohorts and smoothing the averaged images with an 8-mm Gaussian kernel. For PIB, FBB, AV-45, and AV-1451 PET images, 10 typical positive images and 10 typical negative images were selected by an experienced radiologist to make positive and negative template, respectively. For FDG PET images, 10 HC subjects, 10 AD subject, and 10 FTLD subject were used to make an HC FDG template and two dementia-specific FDG templates. For AV-133 PET images, only 10 PD subjects were used to make AV-133 templates for PD subjects, and the AV-133 template for HC subjects was not made because there are only five healthy subjects. For [^{18}F]altanserin, due to the insufficient number of subjects, the template was not made. After constructing the templates, the PET images were spatially normalized by registering with the corresponding templates using SPM12 "Old Normalise" tools. For FDG images of the AD group and FTLD group, both dementia-specific FDG templates and HC FDG template were used to spatially normalize PET images, and the template whose spatially normalized results were closer (higher Pearson correlation coefficient) to those of the MRI-based method was selected for subsequent analysis (HC FDG template for FDG images of the AD group and FTLD-specific FDG template for FDG images of the FTLD group). For each PET image of PIB, FBB, AV-45, and AV-1451, both positive and negative templates were used for spatial normalization, and of the two spatially normalized images, the closer (higher Pearson correlation coefficient) to the gold standard was selected for subsequent analysis.

Atlas-based spatial normalization method

Atlas-based spatial normalization algorithm

The idea of the atlas-based algorithm is to generate the adaptive probabilistic brain atlas that best "matches" the individual PET image from the initial probabilistic brain

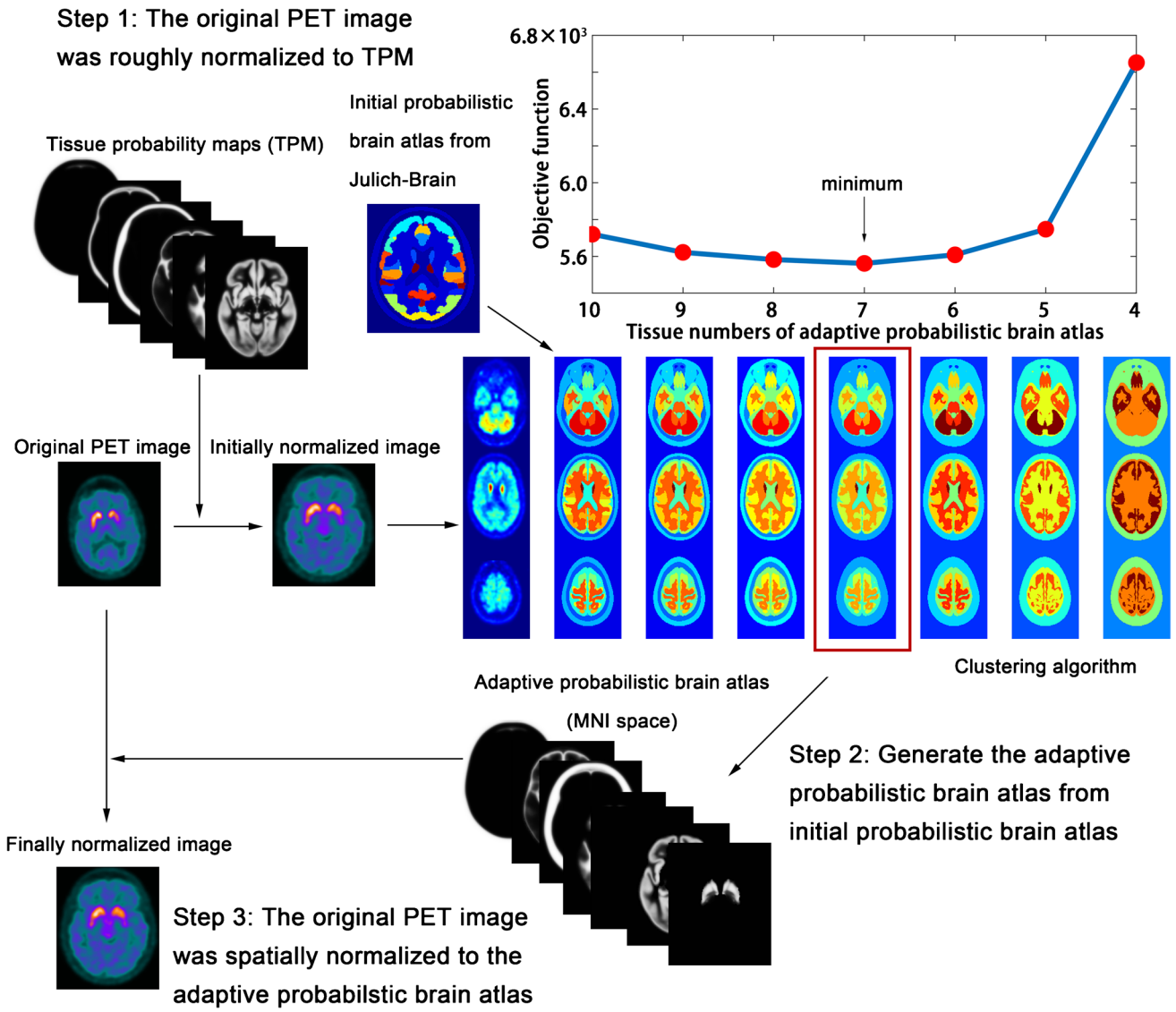

Fig. 1 The flowchart of the atlas-based method

atlas containing fine-grained brain regions, and then register the individual PET image into the adaptive probabilistic brain atlas in MNI space. The adaptive probabilistic brain atlas is a set of probabilistic images for multiple tissue types. The flowchart of the atlas-based spatial normalization algorithm is shown in Fig. 1. First, the unified segmentation algorithm in SPM12 with the TPM (tissue probability maps) of gray matter, white matter, CSF, skin, skull, and background was used to roughly spatially normalize the PET images. Briefly, the unified segmentation algorithm models the signals in the image through Gaussian mixture model and tissue probability maps, and then unifies spatial normalization, segmentation, and nonuniformity correction under a framework of generative model. The optimization of the model parameters is performed using expectation maximization algorithm [10]. Since not all PET images can be simply modeled with the TPM, this step is just used to achieve approximate alignment. Then, the adaptive probabilistic brain atlas generation algorithm was used to generate the adaptive probabilistic brain atlas for each individual PET image. The detailed implementation of the adaptive probabilistic brain atlas generation algorithm is described below. Finally, the unified segmentation algorithm in SPM12 with the adaptive probabilistic brain atlas was used to spatially normalize the PET images.

Adaptive probabilistic brain atlas generation algorithm

In order to generate a corresponding adaptive probabilistic brain atlas for each brain PET image, first, a probabilistic atlas of human brain cytoarchitecture was used as the initial probabilistic atlas. Then, an objective function which reflects the trade-off between the modeling ability and the complexity of atlas was proposed. Finally, a clustering algorithm for merging the brain regions of the initial probabilistic brain atlas was proposed to obtain the adaptive probabilistic brain atlas by minimizing the objective function. Therefore, each time the atlas-based method is performed, a corresponding adaptive probabilistic brain atlas is generated for the target brain PET image.

Initial probabilistic brain atlas

The Julich-Brain, a probabilistic atlas of human brain cytoarchitecture in the MNI space including 91 cortical areas and subcutaneous nuclei, was used as the initial prior information [12]. Due to the finite resolution of PET images, some small brain regions were manually merged into large brain regions based on their anatomical structures to increase the robustness of the algorithm. In addition, since the Julich-Brain does not contain white matter and extra-brain structures, the Julich-Brain and the probability maps of white matter, CSF, skin, and skull were merged together to build a whole probabilistic brain atlas with 41 brain regions.

Objective function

The objective function includes two parts, the likelihood term, which reflects the ability of the atlas to model a brain PET image, and the regularization term, which reflects the complexity of the atlas.

First, the likelihood term of objective function is estimated by a Gaussian mixture model. The weighted mean μ_t and the weighted variance σ_t^2 of voxel intensity in the brain region t are:

$$\mu_t = \sum_{i=1}^{I} \gamma_i^t y_i / \sum_{i=1}^{I} \gamma_i^t$$

$$\sigma_t^2 = \sum_{i=1}^{I} \gamma_i^t (y_i - \mu_t)^2 / \sum_{i=1}^{I} \gamma_i^t$$

where I is the number of voxels in the image, y_i is the intensity of voxel i, and γ_i^t is the prior probability of voxel i belonging to the brain region t, determined by the probabilistic brain atlas. In order to reduce the partial volume effect, we set $\gamma_i^t = 0$ for the voxels on the boundary of the brain regions.

It is assumed that the voxel intensity of PET image in the same brain region satisfies Gaussian distribution. Taking the μ_t and σ_t^2 as the mean and variance of the Gaussian function of intensity distribution in the brain region t, for any voxel i with intensity y_i, the probability density that it belongs to the brain region t is:

$$p_i^t = \gamma_i^t \cdot \frac{1}{\left(2\pi\sigma_t^2\right)^{\frac{1}{2}}} \exp\left(-\frac{\left(y_i - \mu_t\right)^2}{2\sigma_t^2}\right)$$

The probability density that voxel i belongs to the images is the sum of all Gaussians:

$$p_i = \sum_{t=1}^{T} \gamma_i^t \cdot \frac{1}{\left(2\pi\sigma_t^2\right)^{\frac{1}{2}}} \exp\left(-\frac{\left(y_i - \mu_t\right)^2}{2\sigma_t^2}\right)$$

where T is the number of brain regions. Assuming that each voxel is independent, the probability density of the entire image P is the product of the probability densities of all voxels i, $\prod_i p_i$. The assumption that the voxels are independent is to simplify the model and is not rigorous. Take the negative logarithm of P to get the likelihood term:

$$\varepsilon = -\sum_{i=1}^{I} \ln\left(\sum_{t=1}^{T} \frac{\gamma_i^t}{(2\pi\sigma_t^2)^{\frac{1}{2}}} \exp\left(-\frac{(y_i - \mu_t)^2}{2\sigma_t^2}\right)\right)$$

Then, the regularization term of the objective function that reflects the complexity of the model is determined by the number of parameters of the model:

$$l = T * \ln(I)$$

The objective function is the sum of the likelihood term and the regularization term.

$$F = \varepsilon + \lambda * l = -\sum_{i=1}^{I} \ln\left(\sum_{t=1}^{T} \frac{p_i^t}{\left(2\pi\sigma_t^2\right)^{\frac{1}{2}}} \exp\left(-\frac{\left(y_i - \mu_t\right)^2}{2\sigma_t^2}\right)\right) + \lambda * T * \ln(I)$$

where λ is a hyperparameter that can adjust the ratio of the regularization term to the likelihood term.

Clustering algorithm

In order to obtain an adaptive probabilistic brain atlas corresponding to the individual PET brain image, the brain regions of the initial probabilistic brain atlas should be clustered to minimize the objective function. Here, a hierarchical clustering greedy algorithm was proposed:

I Calculate the objective function for the initial atlas and weighted mean of voxel intensity of each brain region.

J Sort the brain regions according to the weighted means from low to high.

K For any brain region, try to merge it with its neighboring brain regions, and calculate the objective function for new atlas. If all the possible merging fails to reduce the objective function, the probabilistic brain atlas at this time is the final result and stop merging. Otherwise, select the merging way which can maximize the reduction of the objective function and generate a new atlas.

L Repeat steps I, J, and K until you get the final adaptive probabilistic brain atlas.

Quantitative verification of atlas-based method

Correlation analysis

All brain PET images in the validation cohort were spatially normalized using three methods (atlas-based, template-based, and MRI-based methods). The intracranial voxels of brain PET images were extracted by the intracranial mask from SPM12. The Pearson correlation coefficients between the voxels of brain PET images computed by MRI-based method and the other two methods were calculated for each image. Paired-sample *t*-tests were then performed to investigate the differences of correlations between template-based and atlas-based method in 14 subgroups (FDG HC, FDG AD, FDG FTLD, PIB HC, PIB AD, PIB FTLD, FBB HC, FBB AD, FBB PD, AV-45 HC, AV-45 AD, AV-1451 HC, AV-1451 AD, and AV-133 PD). $P < 0.05$ was considered statistically significant. The magnitudes of changes in correlation coefficients between the atlas-based and template-based methods versus the MRI-based method across all 14 subgroups were also computed.

Furthermore, the spatial normalization accuracy of atlas-based method was measured by Pearson correlation coefficients between the spatially normalized images obtained by atlas-based method and MRI-based method. The mutual information between the spatially normalized images computed with MRI-based method and the maximum probability maps of the initial probabilistic brain atlas was computed for all images in the validation cohort. Pearson correlation coefficients between the mutual information and spatial normalization accuracy of the 286 PET images and Pearson correlation coefficients between the mean mutual information and mean spatial normalization accuracy of all 16 subgroups of PET images (FDG HC, FDG AD, FDG FTLD, PIB HC, PIB AD, PIB FTLD, FBB HC, FBB AD, FBB PD, AV-45 HC, AV-45 AD, AV-1451 HC, AV-1451 AD, AV-133 HC, AV-133 PD, and [^{18}F]altanserin HC) were computed.

Quantitative comparison at meta-ROI SUVR level

In the clinical trials, meta-ROI SUVRs are usually calculated to indicate the degree of pathology [13]. The meta-ROI SUVR is formed from the voxel average uptake in the meta-ROI normalized to the reference region. The meta-ROIs and reference regions we used for each group are shown in Table S1 in Supplementary File 2. In brief, for AD, the meta-ROI of FDG PET includes the angular gyrus, posterior cingulate, and inferior temporal cortical, and the reference region is the cerebellum [14]. The meta-ROI of tau PET includes the entorhinal, amygdala, parahippocampal, fusiform, inferior temporal, and middle temporal regions, and the reference region is the cerebellar gray matter [13]. For FTLD, the meta-ROI of FDG PET includes the frontal lobe, anterior temporal lobe, and anterior cingulate, and the reference region is the cerebellum [15]. For PD, the meta-ROI of AV-133 PET is the striatum, and the reference region is the occipital lobe [16]. For AD, PD, and FTLD, the meta-ROI for amyloid PET (PIB, FBB, and AV-45) includes the frontal, anterior/posterior cingulate, lateral parietal, and lateral temporal regions, and the reference region is the cerebellum [17].

To evaluate the accuracy of the methods, the relative errors and Pearson correlation coefficients of the meta-ROI SUVRs computed with atlas-based method and template-based method comparing with those computed with MRI-based method were calculated separately for each subject group. To calculate the relative error of meta-ROI SUVRs of a certain method for each group, the relative error of meta-ROI SUVRs for each subject in the group was first calculated, and then the mean and standard error (SEM) of the relative error for all subjects in the group were calculated. The relative error of meta-ROI SUVRs of a certain method in a subject is defined as $\frac{|SUVR_{target\ method} - SUVR_{MRI-based\ method}|}{SUVR_{MRI-based\ method}} \times 100\%$. $SUVR_{target\ method}$ is the meta-ROI SUVR calculated with a certain method (atlas-based method or template-based method).

Voxel-wise SPM analysis

Two-sample *t*-tests and chi-square analysis were first performed on the age and gender of the eight groups (FDG AD vs. HC; FDG FTLD vs. HC; PIB AD vs. HC; PIB FTLD vs. HC; FBB AD vs. HC; FBB PD vs. HC; AV-45 AD vs. HC; AV-1451 AD vs. HC). Voxel-wise two-sample *t*-tests were performed on all eight groups using SPM12 without gender and age as covariates. The pre-processing PET images were performed as follows: The images were spatially normalized into MNI space using atlas-based, template-based, and MRI-based method, smoothed with an 8-mm Gaussian kernel, and intensity normalized to

the reference regions which were same as the reference regions we used to compute meta-ROI SUVRs. The brain regions were considered significant by the GRF correction with voxel-level $P < 0.001$ and cluster-level $P < 0.05$ using DPABI [18]. Therefore, each group will have three different results of the significant changed regions since the difference of the spatial normalization methods. The Dice coefficient was used to compute the similarity between the

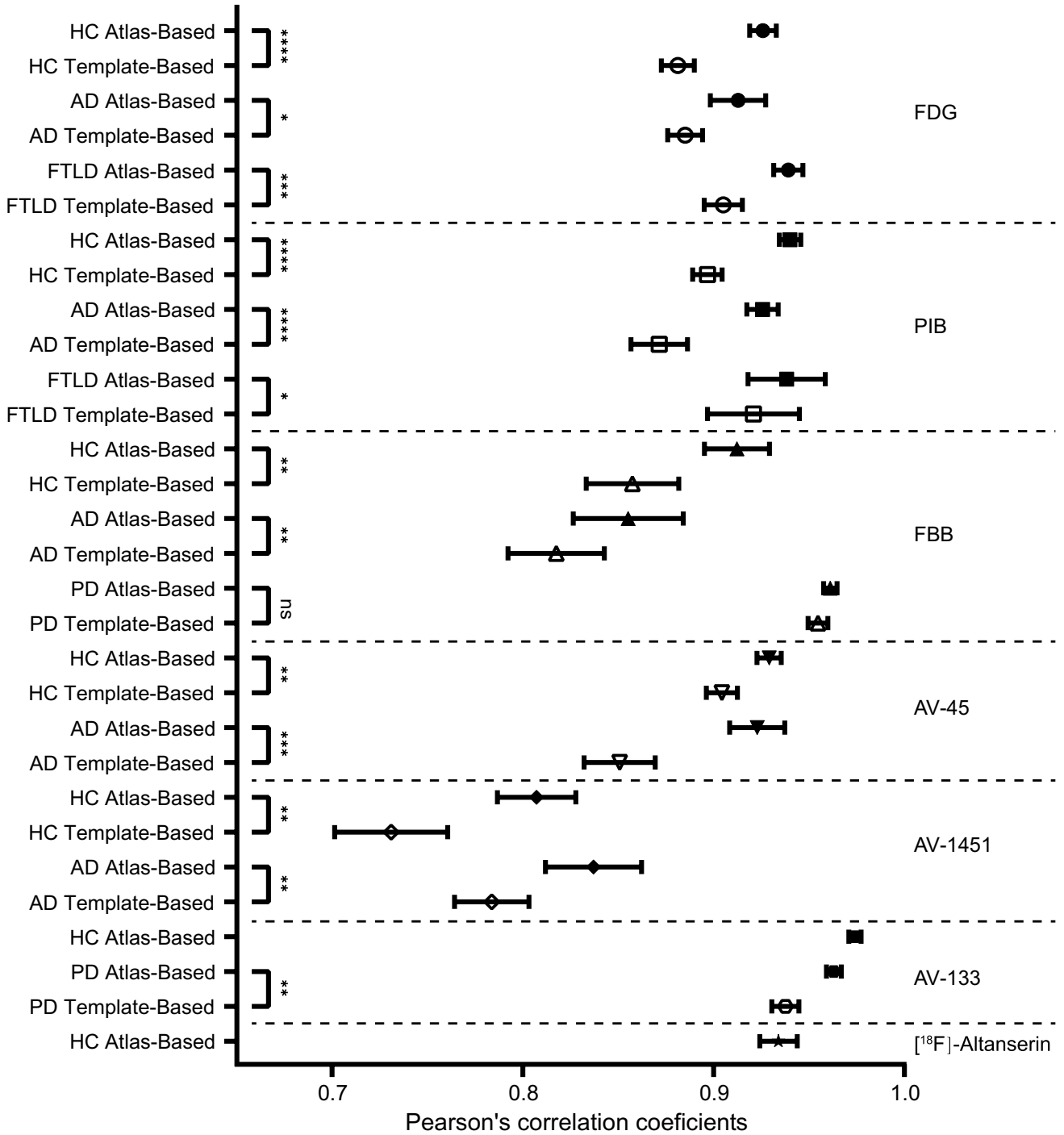

Fig. 2 The Pearson correlation coefficients between the spatially normalized images computed by MRI-based method and the other two (atlas-based and template-based) methods. Paired-sample *t*-tests were then performed to investigate the differences of correlations between template-based and atlas-based method. ns: not significant; $*P < 0.05$; $**P < 0.01$; $***P < 0.001$; $****P < 0.0001$

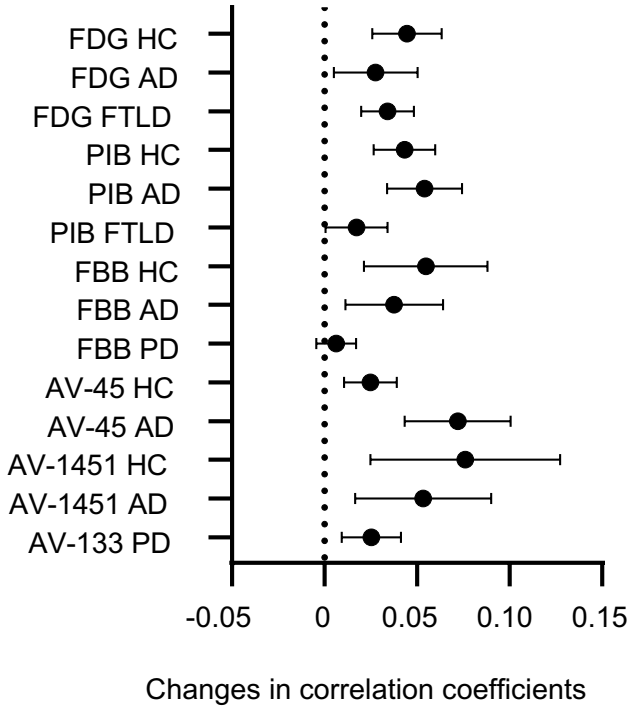

Fig. 3 The changes in correlation coefficients between the atlas-based and template-based methods versus the MRI-based method across all subject groups

results of MRI-based method and the results of the other two methods. The equation for Dice coefficient is:

$$D = \frac{2|A \cap B|}{|A| + |B|}$$

where A and B are two binary masks for the significant brain regions. If the volumes of A and B are 0, we define the Dice coefficient between A and B to be 1.

Result

Correlation analysis

The mean and SEM of Pearson correlation coefficients between the images computed by the MRI-based method and other two methods (atlas-based method and template-based method) were 0.908 ± 0.005 and 0.864 ± 0.006, respectively. The Pearson correlation coefficients of atlas-based method were significantly higher ($P < 0.05$) than those of template-based method in almost all (13/14) groups, as shown in Fig. 2 and Fig. 3.

The mutual information and the spatial normalization accuracy of the atlas-based method were significantly positively correlated, as shown in Fig. 4.

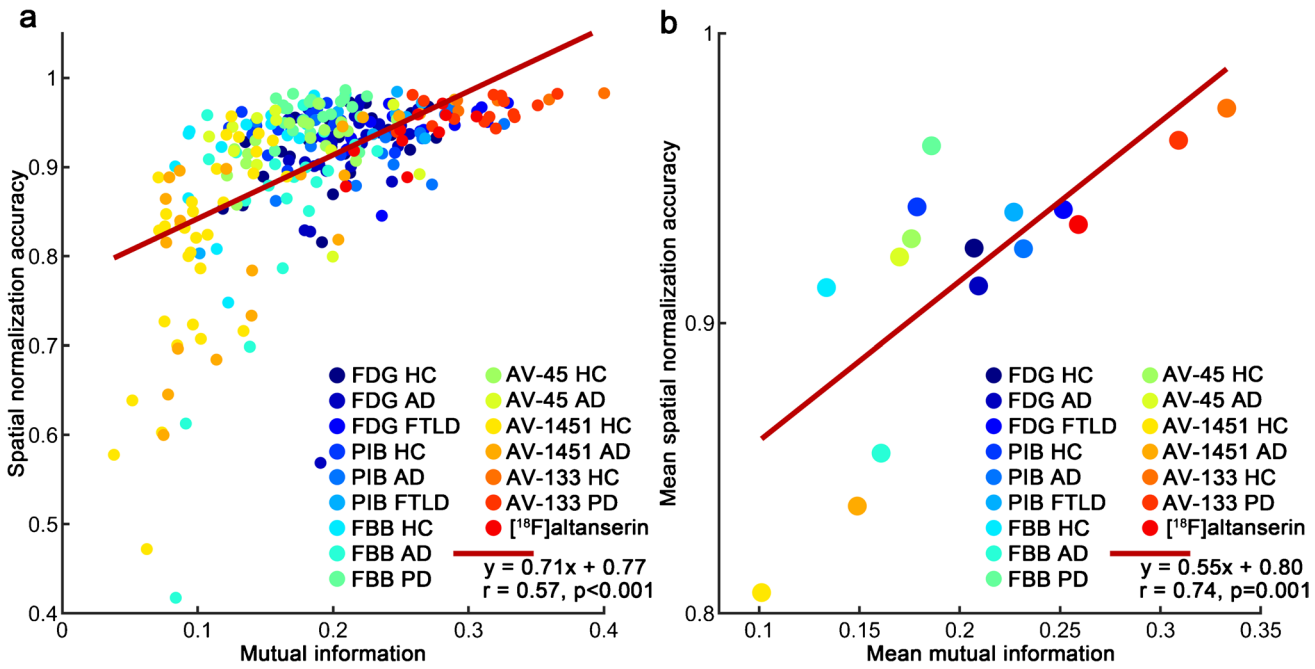

Fig. 4 **a** The correlation between spatial normalization accuracy of atlas-based method and mutual information of the 286 PET images. **b** The correlation between mean spatial normalization accuracy of atlas-based method and mean mutual information of the 16 subgroups of PET images

Quantitative comparison at meta-ROI SUVR level

The mean and SEM of relative errors of meta-ROI SUVR computed with atlas-based method and template-based method were 2.12 ± 0.18% and 3.28 ± 0.24%, respectively. The mean Pearson correlation coefficient of atlas-based method in 15 groups was 0.978 ± 0.005, while the mean Pearson correlation coefficient of template-based method was 0.950 ± 0.012 (see Table 2). Correlations between the meta-ROI SUVR obtained by the MRI-based method and those obtained by the atlas-based or template-based method are shown in Fig. 5.

Voxel-wise SPM analysis

There are no group differences in age and gender between FDG AD groups and FDG HC groups, and between PIB AD groups and PIB HC groups (see Table S2 in Supplementary File 2). The voxel-wise SPM two-sample *t*-test results of FDG AD vs. HC and PIB AD vs. HC are shown in Fig. 6. The SPM results of other groups are shown in Suppl. Figures 1–6 in Supplementary File 2. The Dice coefficients between the significantly different regions computed with atlas-based method and those computed with MRI-based method were higher than the dice coefficients between the significantly different regions computed with template-based method and those computed with MRI-based method in both FDG AD vs. HC groups (0.727 > 0.667) and PIB AD vs. HC groups (0.737 > 0.595).

Discussion

In this study, we proposed a unified spatial normalization method of brain PET images based on the adaptive probabilistic brain atlas. The results showed that the spatially normalized images and the subsequent statistical analysis results obtained with the atlas-based method were highly consistent with those obtained with the MRI-based method. Moreover, the atlas-based method has higher spatial normalization accuracy than the template-based method. Therefore, the atlas-based method allows for accurate registration of brain PET images of different radiotracers and pathological state into standard space without additional structural MR images. Since the atlas-based method is not specifically aimed at the brain PET images of a certain radiotracer, theoretically this method can even be used for the spatial normalization of the brain PET images of the newly developed radiotracer. A MATLAB toolbox for this method is freely available at https://github.com/IHEP-Brain-Imaging/Spatial-Normalization-of-Brain-PET-Images.

The PET images in this study were from multiple datasets with different image protocols. The atlas-based method, however, can be successfully applied to the images from multiple datasets, implying robustness and broad

Table 2 The meta-SUVRs, relative errors, and correlation coefficients obtained by different methods

Groups	Meta-ROI SUVRs *			Relative errors (%) †		Correlation coefficients †	
	MRI-based	Template-based	Atlas-based	Template-based	Atlas-based	Template-based	Atlas-based
FDG HC (AD meta-ROI)	1.003 ± 0.018	1.001 ± 0.015	0.996 ± 0.018	2.22	1.52	0.971	0.985
FDG HC (FTLD meta-ROI)	0.962 ± 0.015	0.943 ± 0.014	0.970 ± 0.015	4.07	2.34	0.855	0.932
FDG AD	0.920 ± 0.017	0.936 ± 0.014	0.916 ± 0.016	2.90	1.21	0.945	0.989
FDG FTLD	0.904 ± 0.046	0.890 ± 0.040	0.933 ± 0.045	3.57	3.65	0.987	0.993
PIB HC	1.133 ± 0.058	1.137 ± 0.064	1.143 ± 0.057	3.79	2.13	0.981	0.993
PIB AD	1.467 ± 0.074	1.501 ± 0.075	1.479 ± 0.073	4.06	2.23	0.967	0.991
PIB FTLD	0.998 ± 0.034	0.992 ± 0.033	1.025 ± 0.034	1.57	2.64	0.969	0.992
FBB HC	1.038 ± 0.020	1.066 ± 0.020	1.049 ± 0.024	3.17	1.46	0.949	0.982
FBB AD	1.451 ± 0.052	1.411 ± 0.045	1.451 ± 0.051	3.54	1.72	0.984	0.984
FBB PD	1.041 ± 0.017	1.056 ± 0.011	1.064 ± 0.015	3.58	2.97	0.867	0.937
AV-45 HC	1.152 ± 0.043	1.166 ± 0.038	1.169 ± 0.042	3.03	1.86	0.977	0.991
AV-45 AD	1.344 ± 0.075	1.294 ± 0.066	1.338 ± 0.071	4.20	1.99	0.975	0.978
AV-1451 HC	1.224 ± 0.015	1.217 ± 0.012	1.214 ± 0.015	2.28	1.50	0.878	0.957
AV-1451 AD	1.498 ± 0.060	1.480 ± 0.059	1.498 ± 0.064	2.25	1.62	0.989	0.989
AV-133 PD	1.640 ± 0.075	1.677 ± 0.064	1.634 ± 0.073	5.03	2.90	0.958	0.982
mean ± SEM	-	-	-	3.28 ± 0.24	2.12 ± 0.18	0.950 ± 0.012	0.978 ± 0.005

*Mean ± SEM

†With MRI-based method

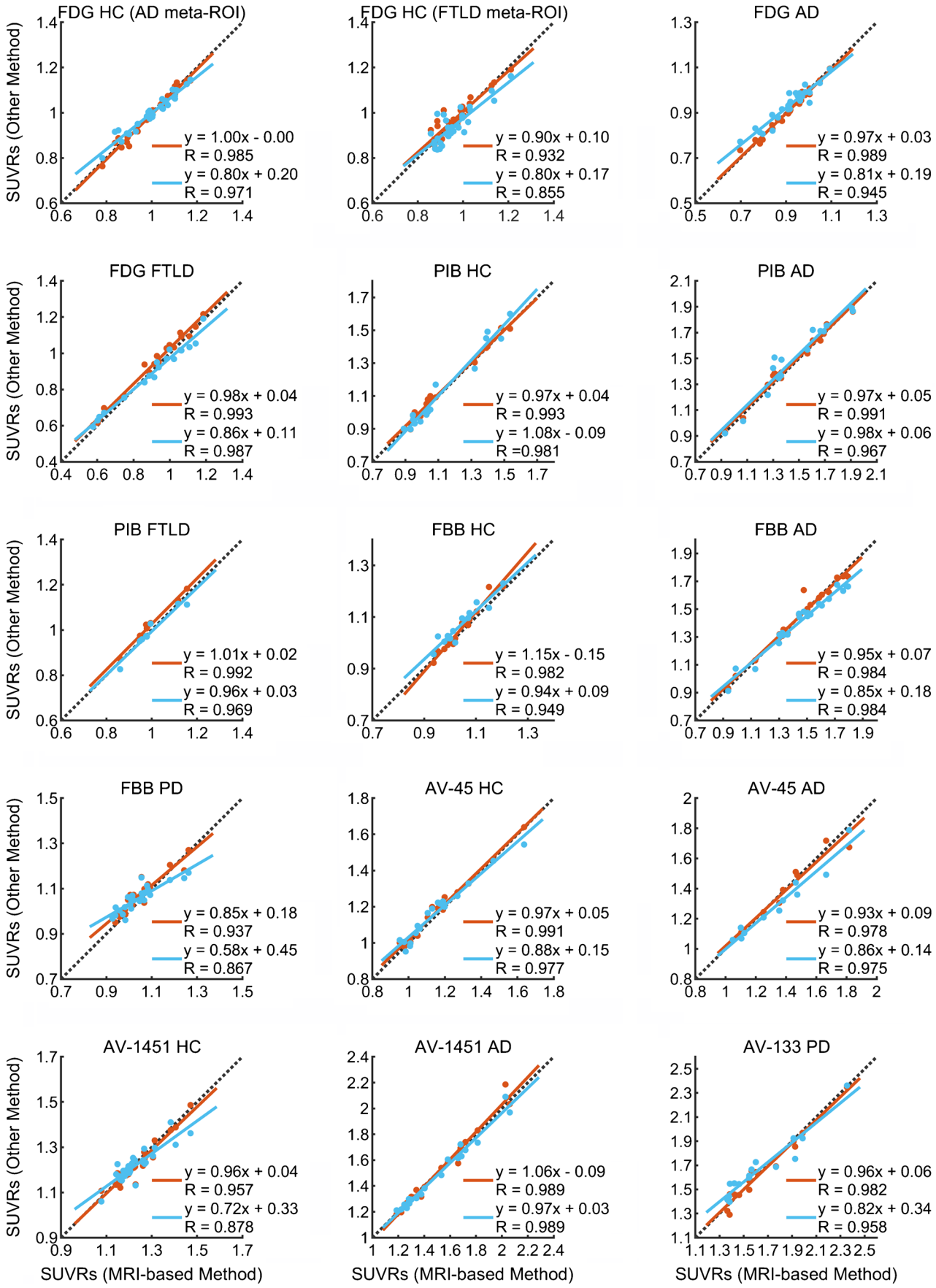
FDG HC (AD meta-ROI)
y = 1.00x - 0.00
R = 0.985
y = 0.80x + 0.20
R = 0.971
FDG HC (FTLD meta-ROI)
y = 0.90x + 0.10
R = 0.932
y = 0.80x + 0.17
R = 0.855
FDG AD
y = 0.97x + 0.03
R = 0.989
y = 0.81x + 0.19
R = 0.945
FDG FTLD
y = 0.98x + 0.04
R = 0.993
y = 0.86x + 0.11
R = 0.987
PIB HC
y = 0.97x + 0.04
R = 0.993
y = 1.08x - 0.09
R =0.981
PIB AD
y = 0.97x + 0.05
R = 0.991
y = 0.98x + 0.06
R = 0.967
PIB FTLD
y = 1.01x + 0.02
R = 0.992
y = 0.96x + 0.03
R = 0.969
FBB HC
y = 1.15x - 0.15
R = 0.982
y = 0.94x + 0.09
R = 0.949
FBB AD
y = 0.95x + 0.07
R = 0.984
y = 0.85x + 0.18
R = 0.984
FBB PD
y = 0.85x + 0.18
R = 0.937
y = 0.58x + 0.45
R = 0.867
AV-45 HC
y = 0.97x + 0.05
R = 0.991
y = 0.88x + 0.15
R = 0.977
AV-45 AD
y = 0.93x + 0.09
R = 0.978
y = 0.86x + 0.14
R = 0.975
AV-1451 HC
y = 0.96x + 0.04
R = 0.957
y = 0.72x + 0.33
R = 0.878
AV-1451 AD
y = 1.06x - 0.09
R = 0.989
y = 0.97x + 0.03
R = 0.989
AV-133 PD
y = 0.96x + 0.06
R = 0.982
y = 0.82x + 0.34
R = 0.958
SUVRs (Other Method)
SUVRs (MRI-based Method)

◂**Fig. 5** Correlations between the meta-ROI SUVRs obtained by the MRI-based method and those obtained by the atlas-based method (red dots and lines) and template-based method (blue dots and lines). The black dotted lines are the lines of identity

applicability of the method. We found that the accuracy of spatial normalization of PET images was positively correlated with the mutual information between the PET images and maximum probability maps of the initial probabilistic brain atlas. Mutual information represents how much information can be gained from one random variable by observing another random variable. On the one hand, this result showed that the accuracy of the spatial normalization is related to the information contained in the image itself. The information contained in the image is related to the tracer, the disease state of the subject, and etc. Therefore, images of different tracers and disease states have different spatial normalization accuracy. On the other hand, since the atlas-based

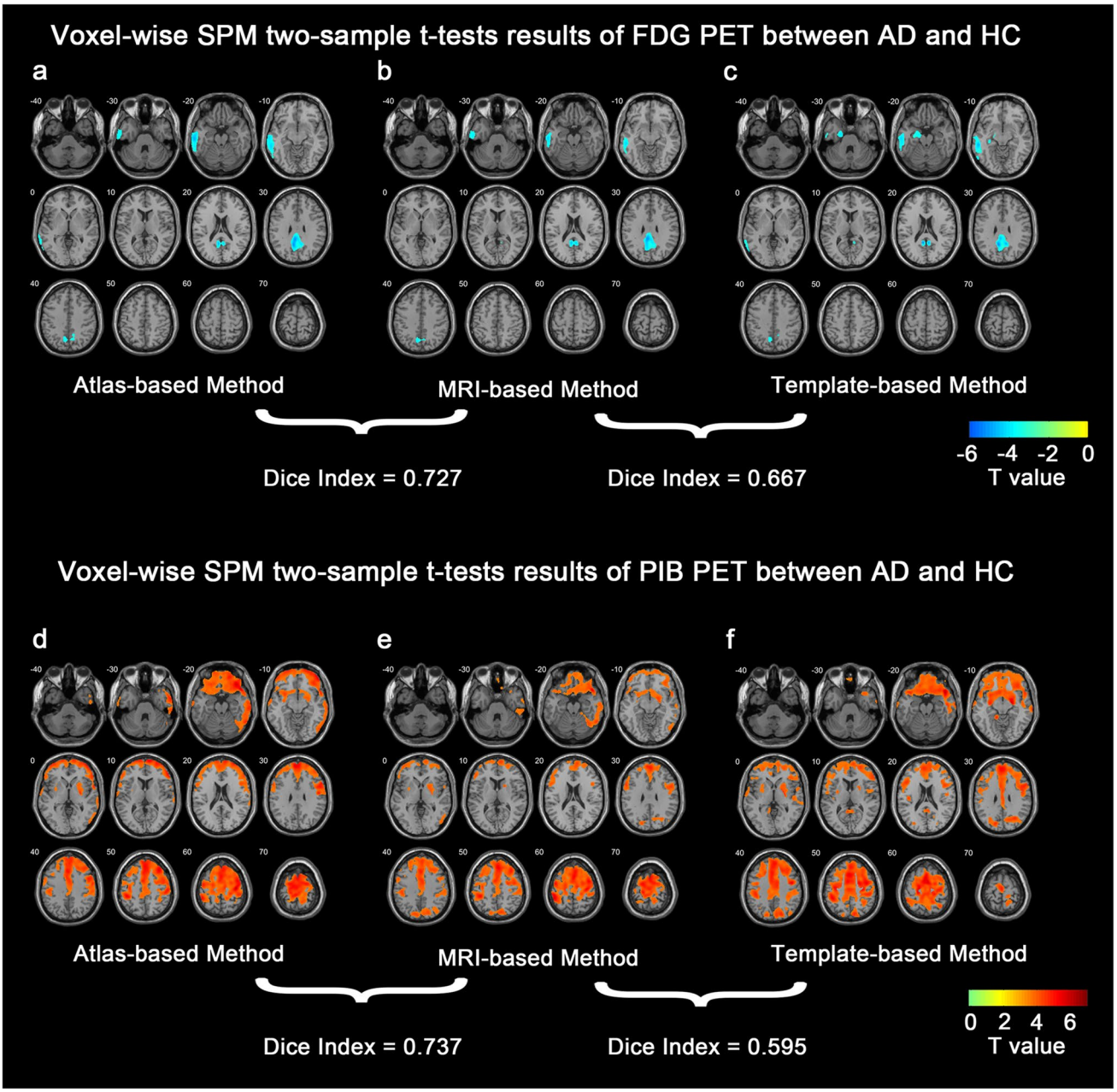

Fig. 6 Voxel-wise SPM results of two-sample *t*-tests of FDG and PIB PET images between AD and HC groups. Significantly (voxel-level $P<0.001$ and cluster-level $P<0.05$, GRF correction) different regions computed with the three methods are shown in **a**-**c** for FDG PET images and in **d**-**f** for PIB PET images

method needs to register the PET image to the adaptive probabilistic brain atlas, the probabilistic brain atlas is crucial for PET image spatial normalization accuracy. The brain atlas used in this study is probabilistic, which enables it to account for variations between individual brains. However, due to the atrophy and deformation of the brain in patients, the spatial normalization accuracy of PET images of patients may be further improved by making patient-specific probabilistic brain atlas. The template-based method was treated as a control method in this study. Many studies have constructed different templates for different brain PET images. For example, positive and negative tau PET templates were constructed by using 24 AD patients and 22 HC subjects [7]. A PIB PET template suitable for Down syndrome patients was constructed using 72 patients [6]. Positive, negative, and mixed PIB PET templates suitable for AD and HC were also created [8]. Therefore, we also made positive and negative templates for PIB, FBB, AV-45, and AV-1451 PET images. One problem of the template-based method is that it is necessary to select a suitable template before registration, so that the template-based method is subjective. In this study, we picked the template based on the spatial normalization results of MRI-based methods, so that we could reach the "best" results of the template-based method. The atlas-based method, however, avoids the subjectivity of the researchers and makes the results more reproducible.

Other kinds of PET-only methods have been proposed. One way is using adaptive templates to spatially normalize PET images of PIB [19] or ^{18}F-flutemetamol [20, 21]. These methods use a linear combination of two images to generate an adaptive template that spans the uptake range from the most negative amyloid-β image to the most positive amyloid-β image. Therefore, these methods are limited to the spatial normalization of amyloid-β imaging. By comparison, the atlas-based method can be applied not only to amyloid-β imaging, but also to brain PET images of other radiotracers. Deep learning has also been used for PET image spatial normalization. For example, a deep neural network for spatial normalization of tau PET images was trained and validated using 199 tau PET images and corresponding MR images [22]. Two deep neural networks that produce adaptive PET templates for PIB PET images were trained and validated using 681 pairs of simultaneously acquired PIB PET and MRI scans of AD, MCI, and HC subjects [23]. These methods usually require hundreds of PET images and the corresponding MR images to train deep neural networks, and the trained neural network can only be used for the brain PET images of a specific radiotracer depending on the training data. Collecting hundreds of thousands of brain PET images of a specific tracer and their corresponding MR images to train deep neural networks is difficult, expensive, and time-consuming for some clinical studies. The atlas-based method, however, does not require any PET images or MR images for training, and can be used for spatial normalization of the PET images of multiple radiotracers.

There are some limitations in the atlas-based method. First, the origin and direction of the images will affect the results. This is due to the nature of the unified segmentation algorithm. Therefore, the origin of the image should be placed close to the anterior commissure and the direction of the image should be positioned to roughly match MNI space before performing the atlas-based method. Second, the atlas-based method is currently validated on PET images of 7 common radiotracers. Although our method is applicable to almost all kinds of brain PET images in principle, it needs further verification on other radiotracers.

Conclusion

In this study, we proposed a unified method for accurate spatial normalization of various brain PET images without MR images, and the method has potential clinical applications.

Supplementary Information The online version contains supplementary material available at https://doi.org/10.1007/s00259-022-05752-6.

Acknowledgements Data used in preparation of this article were obtained from the Alzheimer's Disease Neuroimaging Initiative (ADNI) database (adni.loni.usc.edu). As such, the investigators within the ADNI contributed to the design and implementation of ADNI and/or provided data but did not participate in analysis or writing of this report. A complete listing of ADNI investigators can be found at: http://adni.loni.usc.edu/wp-content/uploads/how_to_apply/ADNI_Acknowledgement_List.pdf.

Author contribution Data processing and analysis were performed by Tianhao Zhang and Hua Liu. The design of the algorithm was performed by Tianhao Zhang, Baoci Shan, and Binbin Nie. The first draft of the manuscript was written by Tianhao Zhang and all authors commented on previous versions of the manuscript. All authors read and approved the final manuscript.

Funding This work was financially supported by the China Postdoctoral Science Foundation (2021T140668) and National Natural Science Foundation of China (11975249, 81771923, 12175268).

Data availability The data used in the current study come from five public datasets: ADNI (Alzheimer's Disease Neuroimaging Initiative; http://adni.loni.usc.edu), AIBL (The Australian Imaging, Biomarker and Lifestyle Study of Aging; http://www.AIBL.csiro.au), ICBM (International Consortium for Brain Mapping), NIFD (Neuroimaging in Frontotemporal Dementia; https://memory.ucsf.edu/research-trials/research/allftd), and PPMI (Parkinson's Progression Markers Initiative; https://www.ppmi-info.org). The codes and templates for this study are available at https://github.com/IHEP-Brain-Imaging/Spatial-Normalization-of-Brain-PET-Images.

Declarations

Competing interests The authors declare no competing interests.

References

1. Hooker JM, Carson RE. Human positron emission tomography neuroimaging. In: Yamush ML, editor. Annual Review of Biomedical Engineering, Vol 21; 2019. p. 551–81.
2. Zimmer L, Luxen A. PET radiotracers for molecular imaging in the brain: past, present and future. Neuroimage. 2012;61:363–70. https://doi.org/10.1016/j.neuroimage.2011.12.037.
3. Gupta S, Gupta P, Verma VS. Study on anatomical and functional medical image registration methods. Neurocomputing. 2021;452:534–48. https://doi.org/10.1016/j.neucom.2020.08.085.
4. Bourgeat P, Villemagne VL, Dore V, Brown B, Macaulay SL, Martins R, et al. Comparison of MR-less PiB SUVR quantification methods. Neurobiol Aging. 2015;36:S159–66. https://doi.org/10.1016/j.neurobiolaging.2014.04.033.
5. Meyer JH, Gunn RN, Myers R, Grasby PM. Assessment of spatial normalization of PET ligand images using ligand-specific templates. Neuroimage. 1999;9:545–53. https://doi.org/10.1006/nimg.1999.0431.
6. Lao PJ, Handen BL, Betthauser TJ, Cody KA, Cohen AD, Tudorascu DL, et al. Imaging neurodegeneration in Down syndrome: brain templates for amyloid burden and tissue segmentation. Brain Imaging Behav. 2019;13:345–53. https://doi.org/10.1007/s11682-018-9888-y.
7. Sun X, Liang SX, Fu LP, Zhang XJ, Feng T, Li PL, et al. A human brain tau PET template in MNI space for the voxel-wise analysis of Alzheimer's disease. J Neurosci Methods. 2019;328:8. https://doi.org/10.1016/j.jneumeth.2019.108438.
8. Chae SY, Kim HO, Oh M, Lee DY, Jin S, Oh SJ, et al. Evaluation of selective positron emission tomography template method for spatial normalization of amyloid imaging with C-11-Pittsburgh compound B. J Comput Assist Tomogr. 2014;38:924–9.
9. Martino ME, de Villoria JG, Lacalle-Aurioles M, Olazaran J, Cruz I, Navarro E, et al. Comparison of different methods of spatial normalization of FDG-PET brain images in the voxel-wise analysis of MCI patients and controls. Ann Nucl Med. 2013;27:600–9. https://doi.org/10.1007/s12149-013-0723-7.
10. Ashburner J, Friston KJ. Unified segmentation. Neuroimage. 2005;26:839–51. https://doi.org/10.1016/j.neuroimage.2005.02.018.
11. Mazziotta J, Toga A, Evans A, Fox P, Lancaster J, Zilles K, et al. A probabilistic atlas and reference system for the human brain: International Consortium for Brain Mapping (ICBM). Philos Trans R Soc B Biol Sci. 2001;356:1293–322. https://doi.org/10.1098/rstb.2001.0915.
12 Amunts K, Mohlberg H, Bludau S, Zilles K. Julich-Brain: a 3D probabilistic atlas of the human brain's cytoarchitecture. Science. 2020;369:988-+. https://doi.org/10.1126/science.abb4588.
13. Jack CR, Wiste HJ, Weigand SD, Therneau TM, Lowe VJ, Knopman DS, et al. Defining imaging biomarker cut points for brain aging and Alzheimer's disease. Alzheimers Dementia. 2017;13:205–16. https://doi.org/10.1016/j.jalz.2016.08.005.
14. Landau SM, Harvey D, Madison CM, Koeppe RA, Reiman EM, Foster NL, et al. Associations between cognitive, functional, and FDG-PET measures of decline in AD and MCI. Neurobiol Aging. 2011;32:1207–18. https://doi.org/10.1016/j.neurobiolaging.2009.07.002.
15. Brown RKJ, Bohnen NI, Wong KK, Minoshima S, Frey KA. Brain PET in suspected dementia: patterns of altered FDG metabolism. Radiographics. 2014;34:684–701. https://doi.org/10.1148/rg.343135065.
16. Gao R, Zhang GJ, Chen XQ, Yang AM, Smith G, Wong DF, et al. CSF biomarkers and its associations with F-18-AV133 cerebral VMAT2 binding in Parkinson's disease-a preliminary report. Plos One. 2016;11. https://doi.org/10.1371/journal.pone.0164762.
17. Landau SM, Breault C, Joshi AD, Pontecorvo M, Mathis CA, Jagust WJ, et al. Amyloid-beta imaging with Pittsburgh compound B and florbetapir: comparing radiotracers and quantification methods. J Nucl Med. 2013;54:70–7. https://doi.org/10.2967/jnumed.112.109009.
18. Yan CG, Wang XD, Zuo XN, Zang YF. DPABI: data processing & analysis for (resting-state) brain imaging. Neuroinformatics. 2016;14:339–51. https://doi.org/10.1007/s12021-016-9299-4.
19. Fripp J, Bourgeat P, Raniga P, Acosta O, Villemagne V, Jones G, et al. MR-less high dimensional spatial normalization of C-11 PiB PET images on a population of elderly, mild cognitive impaired and Alzheimer disease patients. 11th International Conference on Medical Image Computing and Computer-Assisted Intervention (MICCAI2008). New York, NY; 2008. p. 442-+.
20. Lundqvist R, Lilja J, Thomas BA, Lotjonen J, Villemagne VL, Rowe CC, et al. Implementation and validation of an adaptive template registration method for F-18-flutemetamol imaging data. J Nucl Med. 2013;54:1472–8. https://doi.org/10.2967/jnumed.112.115006.
21. Lilja J, Leuzy A, Chiotis K, Savitcheva I, Sorensen J, Nordberg A. Spatial normalization of F-18-flutemetamol PET images using an adaptive principal-component template. J Nucl Med. 2019;60:285–91. https://doi.org/10.2967/jnumed.118.207811.
22. Alven J, Heurling K, Smith R, Strandberg O, Scholl M, Hansson O, et al. A deep learning approach to MR-less spatial normalization for tau PET images. 10th International Workshop on Machine Learning in Medical Imaging (MLMI) / 22nd International Conference on Medical Image Computing and Computer-Assisted Intervention (MICCAI). Shenzhen, PEOPLES R CHINA: Springer International Publishing Ag; 2019. p. 355–63.
23. Kang SK, Seo S, Shin SA, Byun MS, Lee DY, Kim YK, et al. Adaptive template generation for amyloid PET using a deep learning approach. Hum Brain Mapp. 2018;39:3769–78. https://doi.org/10.1002/hbm.24210.